

Enhanced flood mapping using synthetic aperture radar (SAR) images, hydraulic modelling, and social media: A case study of Hurricane Harvey (Houston, TX)

Vincenzo Scotti^{1,2}  | Mario Giannini¹ | Francesco Cioffi¹

¹Department of Civil, Constructional and Environmental Engineering, Sapienza University of Rome, Rome, Italy

²e-GEOS – Product Management Division – Italian Space Agency/Telespazio, Rome, Italy

Correspondence

Prof. Francesco Cioffi, Department of Civil, Constructional and Environmental Engineering, Sapienza University of Rome, 001841 Rome, Italy.
Email: francesco.cioffi@uniroma1.it

Abstract

Post event flooding maps are currently extracted from synthetic-aperture radar (SAR) and/or optical satellite images or developing using hydraulic model simulations. Several sources of uncertainties impact the accuracy of such flood maps constructed from each method, especially in urban areas. An integrated approach that combines satellite images of flooded areas, hydraulic models, and markers from social media that should reduce these uncertainties and allow a more accurate reconstruction of flooded urban areas, is presented in this paper. The flooding associated with Hurricane Harvey in Houston, TX was chosen as a case study. Model validations demonstrate the effectiveness of our integrated approach in reconstructing an accurate flooding map, as well as the temporal and spatial patterns of flooding. Using the experience from this case study we discuss the possibility to use satellite data, instead of ground-based rainfall gauge measurements as precipitation inputs to the hydraulic model; and possible error sources in simulating flooding in urban areas using the hydraulic model.

KEYWORDS

emergency, extreme events, hydraulic modelling, management, remote sensing

1 | INTRODUCTION

Post-event flood maps are typically built using algorithms that detect inundated areas by satellite images or through the use of simulations by hydraulic models. More recently, social markers, such as photos taken during the event and posted on social media, are also used.

The most common satellite sensors for detection of inundated areas are synthetic-aperture radar (SAR), Interferometric synthetic aperture radar (InSAR), or optical channels. Flooding is typically recognised in SAR using the change detection (CD) technique (Aunirundronkool

et al., 2012), in InSAR by interferometric coherence (D'Addabbo, Refice, Lovergine, & Pasquariello, 2017; Pulvirenti, Chini, Pierdicca, & Boni, 2016), and combining optical channel images with a high-resolution DEM (Irwin, Beaulne, Braun, & Fotopoulos, 2017; Liu, Sahli, Meng, Huang, & Lin, 2017).

Each of these satellite-based methods has significant limitations in identifying the flooded area. Using SAR and CD is challenging in the presence of dense vegetation and of shadows; the high roughness of the ground (Brivio, Colombo, Maggi, & Tomasoni, 2002; Giustarini et al., 2013), and atmospheric disturbances (Cian,

This is an open access article under the terms of the Creative Commons Attribution License, which permits use, distribution and reproduction in any medium, provided the original work is properly cited.

© 2020 The Authors. *Journal of Flood Risk Management* published by Chartered Institution of Water and Environmental Management and John Wiley & Sons Ltd.

Marconcini, Ceccato, & Giupponi, 2018) that accompany extreme rainfall events. A main problem for InSAR-based methods is the lack of availability of databases containing multitemporal and interferometric images. Furthermore, often “false positives and negatives errors” (Chini et al., 2016; Ferretti, Prati, & Rocca, 2001; Refice et al., 2014) are a problem for an image. These errors are common in urban areas or where there is water under the vegetation. Finally, methods using an optical sensor with a DEM, do not provide useful information in the presence of clouds (Carincotte, Derrode, & Bourennane, 2006).

There are several constellations of radar satellites whose high-resolution images are used to obtain flooding maps, such as Sentinel 1 (S1), ICEYE, Cosmo Skymed (CSK) and Terrasar X (TSX). Only, the S1 constellation provides free, global images with constant revisit times. In contrast, ICEYE acquires globally and continuously but its data are not freely accessible. TSX and CSK are neither freely accessible nor systematically acquired at global scale (Cian et al., 2018). Another limitation, common to all the radar satellites, is the time lag between the flood occurrence and the availability of the measurements (Di Baldassarre et al., 2009). Usually, the delivery of images can be obtained after 24–48 hours from the extreme event (Schumann, Bates, Horritt, Matgen, & Pappenberger, 2009).

Hydrodynamic models compute floodplain inundations by solving the hydrodynamic equations of motion for given geometries, hydraulic boundaries and initial conditions (Fohringer, Dransch, Kreibich, & Schröter, 2015). In order to simulate hydraulic flow conditions occurring during flooding events, models must also be able to simulate wet and dry conditions, supercritical and subcritical flows and their transition, and allow the direct application of rainfall.

Usually, model simulations are carried out by a combined one dimensional/two dimensional approach in which river flow is assumed one dimensional while two-dimensional flow is considered in the surrounding floodplain (Leandro, Chen, Djordjević, & Savić, 2009; Mazzoleni et al., 2014). The two-dimensional approach integrates shallow water motion equations, (Costabile & Macchione, 2012; Proust, Bousmar, Riviere, Paquier, & Zech, 2010). Three-dimensional or quasi-three-dimensional ones (Orton et al. 2012) methods have also been used. Computation time depends on the spatial resolution (Falter et al., 2013) and on the numerical algorithms used for integrating the model equations (Horritt & Bates, 2001).

The two-dimensional approach is preferred when the flood must be simulated on a large scale (more than 10,000 km²) (Alcrudo & Garcia-Navarro, 1993; Anastasiou & Chan, 1997; Hunter et al., 2008; Liand, Borthwick, & Stelling, 2014; Mignot, Paquier, & Haider, 2006; Mingham &

Causon, 1998; Toro, 2001). Model simulations provide flow depth, velocity and hence the flooding extension, that are fundamental quantities for damage assessment (Grigg & Helweg, 1975).

Several sources of uncertainties affect the accuracy of flooding maps obtained by model simulation. These include difficulties in model calibration and validation due to scarcity of the hydrological data and inaccuracies in representing flow resistance factors, due to the complex interaction of the flow with the structures as, for example, buildings (Bales & Wagner, 2009; Di Baldassarre & Montanari, 2009; Di Baldassarre, Schumann, Bates, Freer, & Beven, 2010; Domeneghetti, Vorogushyn, Castellarin, Merz, & Brath, 2013; Dottori, Di Baldassarre, & Todini, 2013; Grimaldi, Petroselli, Arcangeletti, & Nardi, 2013; Jung & Merwade, 2015). To represent such complex flow features, a very high spatial resolution computational mesh and high computational time would be required. To limit the computational time, a sub-grid approach is applied to a coarser grid (Balzano, 1998; Bates & Hervouet, 1999; Casulli, 2009, Defina, 2000, Viero, Peruzzo, Carniello, & Defina, 2014). Such an approach is applied to model effects such as overland flow over irregular topography (Defina, 2000), roughness and topographic effects based on LiDAR data (Casas, Lane, Yu, & Benito, 2010), additional friction due to emerging vegetation (Mason et al., 2003), inundation of urban areas (McMillan & Brasington, 2007; Sanders, Schubert, & Gallegos, 2008; Yu & Lane, 2006), river hydraulics over large areas and data sparse areas (Neal et al., 2015; Neal, Schumann, & Bates, 2012), and coupled hydrological-hydrodynamic simulations in low-land catchments (Viero et al., 2014).

Social media markers are a new source of information that could be useful to manage a flooding emergency (de Bruijn, de Moel, Jongman, Wagemaker, & Aerts, 2018; Li, Wang, Emrich, & Guo, 2018; Li, 2017; Poser & Dransch, 2010; Rosser, Leibovici, & Jackson, 2017; Smith, Liang, James, & Lin, 2017; Wang, Mao, Wang, Rae, & Shaw, 2018). They are also useful for post event, rapid flooding mapping, as they can provide timely localised information about water depth of inundated areas and damages (Fohringer et al., 2015). However, errors affect the quantitative assessment of flooding by social markers. These can be due to differences between the place where the photo is taken and the location of the tweet posted online, as well as, an incorrect photo-interpretations of the photo perspective. Such errors could be reduced by combining high resolution DEM and social markers (Mandlbürger, Hauer, Höfle, Habersack, & Pfeifer, 2009). A generalised use of social markers makes it necessary to filter a huge amount of information from social media. Recently, several approaches have been pursued. These

include: (a) filtering by keywords or by geographic queries (Rogstadius, Kostakos, & Laredo, 2011 or Joseph et al., 2014), (b) filtering by crowdsourcing (Howe, 2006), (c) automatic filtering utilising machine learning and natural language processing (Sakaki, Okazaki, & Matsuo, 2010); Yin, Lampert, Cameron, Robinson, & Power, 2012) and (d) interactive visual spatiotemporal analysis/geovisual analytics (MacEachren et al., 2011); Morstatter, Kumar, Liu, & Maciejewski, 2013). None of such approaches is completely satisfying, and often a rather empirical post-processing phase which involves a subjective judgement of the operator is required.

Also video cameras, ever increasing in urban areas, may be an useful tool for the civil protection and flood defence purposes (Chang & Guo, 2006; Filonenko, Hernández, Seo, & Jo, 2015; Lopez-Fuentes, Rossi, & Skinnemoen, 2017; Tauro, Olivieri, Petroselli, Porfiri, & Grimaldi, 2016). This could suggest the integration of the information derived from social media markers with those derived from their records. Unfortunately, the access to this source of information is difficult due to privacy concerns.

The uncertainties in developing accurate post event flooding maps, for each of the described approaches separately, motivate an integrated approach based on the combined use of remote sensing from satellites for the delineation of flooding, a hydraulic model for the reconstruction of flooding flow evolution and, finally, social markers in those areas where remote sensing fails and for the validation of hydraulic model results.

In this paper, we integrate the different approaches through the following steps: (a) we use the flooding maps indicated by satellite images to calibrate the hydraulic model; (b) reconstruct the flooding characteristics (i.e., flow depth and velocity) in the urban area by simulation from a calibrated hydraulic model; and (c) validate the model simulations within the urban areas, on the basis of the hydraulic characteristics of the flow (e.g., the water depth) inferred by the social markers. Due to the limitation of satellite images to capture flooding in urban areas, only the flooded suburban or rural areas can be used to calibrate the hydraulic model.

We apply our approach to the reconstruction of the serious flooding occurred in the Houston region due to the Harvey hurricane. Harvey, a hurricane of category 4, hit South-eastern Texas between August 25th and 31st of 2017, with catastrophic rains, which caused major flooding in Houston and its low-lying surrounding areas. Hurricane Harvey generated the largest rainfall of any U.S. hurricane on record. Heavy rains scattered over the territory with a 1,270 mm total rainfall amount. On August 27th, a maximum daily rainfall amount of 760 mm was observed. The highest rainfall

amount was recorded at Galveston Bay, Houston, with over 1,016 mm of rain in 48 hours (NWS, 2017). Over 20,000 people were forced to seek emergency shelter during the event and an estimated 120,000 structures were affected by flooding. Emanuel (2017) estimated a return period of Hurricane Harvey's rainfall to be around a once in 2,000 yr event. The same author, using climatic projections from general circulation models (GCM), has shown as the return period of the event (storm total rainfall greater than 500 mm) reduces to a once in 100 yr by the end of this century. The increasing probability of occurrence of such extreme rainfall events - also highlighted by others authors (e.g., Van Oldenborgh et al. (2017) - suggests the importance of carrying out accurate post-event flooding maps to identify and design measures and infrastructures to mitigate future more frequent extreme floods.

A further motivation for the choice of such case study, beyond the exceptional hydrological event, is that Houston is equipped with a large number of rainfall and streamflow stations, which provide the data for the validation of the approach. A 2D hydraulic model from the USACE Hydrologic Engineering Center's River Analysis System (HEC-RAS 5.0.7) was used. It meets the minimum requirements of National Flood Insurance Program as required by FEMA. We explore how the spatial resolution of the mesh affects the accuracy of model simulations. Finally, we examine whether remote sensing can be useful, in the case of non-instrumented areas, in the retrieval of hydrological data (e.g., precipitation) as input of hydraulic models.

2 | METHODS AND DATA

2.1 | Methods

The main goal of the study is to explore the possibility to obtain an accurate post-event flooding map integrating data extracted by satellite images, social markers and hydraulic numerical model simulations. In particular we are interested in obtaining an accurate reconstruction of flow characteristics (depth and velocity) within urban areas, which, as underlined in the introduction, are not detected by satellite images and difficult to calculate by numerical models.

The idea, to overcome the above limitations, is to calibrate the numerical model using the flooding areas detected in suburban or rural areas, where the satellite images provide reliable records of flooding, and then to infer the flow depth and velocity within the urban areas from the hydraulic simulations by the calibrated model.

The saturation factor k as defined by Şen (2008) was assumed as calibration parameter.

$$\frac{dR}{dP} = (1 - e^{-kP}) \quad (1)$$

where $\frac{dR}{dP}$ is the runoff rate, being R the runoff and P the precipitation amount. Typically the value of k is depending on the land cover and of hydrologic soil group (Table 1).

In the present study case uniform values of k were assumed for the entire integration domain. To calibrate k , the fit between the flooding areas detected by satellite images A_{obs} and those obtained by mathematical simulations A_{sim} , the following index was used:

$$I(k) = \frac{A_{obs} \cap A_{sim}(k)}{A_{obs} \cup A_{sim}(k)} \quad (2)$$

The best value of the saturation factor k was identified as the one that yields the maximum value of $I(k)$. In Equation (2) A_{sim} refers only to the flooding areas which are detected by satellite. We select such flooded areas on the basis of land-cover types. Specifically, we do not include areas belonging to urban and forest land cover types. To validate model simulations within the urban

areas, we use flow depths obtained by social markers which provide photographs or records of the flooding event at specific location and time.

The rainfall data recorded from the rain gauges located in the Houston area, as well as the record of storm surge along the coast are used as model inputs. We also use hydrometric data from streamflow stations as further validation elements.

Houston is a particularly well monitored region. In order to assess if such approach can be extended to non-instrumental areas (i.e., regions in which we can use only satellite data and social markers, and where rainfall and streamflow gauge data are lacking) we analysed a case in which rainfall data from ground-based gauges are not available (Beck et al., 2017; Omranian & Sharif, 2018; Sun et al., 2018; Tan & Santo, 2018) by considering only the satellite based rainfall data. This way we could verify if the rainfall data derived by satellite data were sufficiently reliable to perform a post-event flooding mapping. The data resolution in the area of Houston city, was $0.1^\circ \times 0.1^\circ$, latitude and longitude.

Finally, to verify whether the use of subgrid approach (Casulli, 2009) for simulating flow in urban areas, which is applied in HEC-RAS model, might allow to use coarser mesh size, thus reducing the model computation time, a sensitivity analysis of the possible errors on simulated flow variables due to a reduction of the spatial resolution of the computational mesh was carried out.

TABLE 1 Catchment descriptions and k values in mm^{-1} , adapted from Şen (2008)

Land use description	Cover description	k range values (mm^{-1})
Agricultural	Row crops	0.006–0.018
Commercial	Urban districts: Commercial and business	0.019–0.062
Forest	Woods	0.001–0.011
Grass/pasture	Pasture, grassland	0.002–0.013
High density residential	Residential districts by average lot size	0.006–0.062
Industrial	Urban district: Industrial	0.008–0.043
Low density residential	Residential districts by average lot size	0.001–0.019
Open spaces	Open space lawns, parks, golf courses, cemeteries, etc.	0.003–0.017
Parking and paved spaces	Impervious areas: paved parking lots, roofs, driveways, etc. excluding right-of-way	0.160–0.320
Water/wetlands		0

2.2 | Hydrological data

The hydrological data used in the study refer to: (a) measured rainfall amount at different rain gauges within the Huston areas; (b) measured hydrometric levels at the streamflow gauges of drainage network; (c) precipitation derived by satellite data by CHIRPS (rainfall estimates from rain gauge and satellite observations), NCEP-CPC (National Center for Environmental Prediction - Climate Prediction Center), NCEP-GOB (National Center for Environmental Prediction—Global observation), TRMM-3B42 (tropical rainfall measuring mission) and GPM-IMERG (global precipitation measurements). Data sources are reported in Table 2.

Rainfall amounts and water levels in bayous and major streams in Houston, recorded during 20/08–01/09 with a resolution of 15 minutes, were obtained by Harris County Flood Control District's Flood Warning System (www.harriscountyfws.org). Storm surge levels during the events were downloaded by the site <http://www.ioc-sealevelmonitoring.org/map.php>. Measurements of the sea level were obtained from the Harris County Flood Warning System (www.harriscountyfws.org).

2.3 | SAR images

SAR Satellite images, were downloaded from the Copernicus website (<http://emergency.copernicus.eu>).

Flooding maps were performed by change detection (CD) technique applied on high-resolution X-band images (from 1 to 4 m) of the Italian COSMO-SkyMed

constellation (Chini, Pulvirenti, & Pierdicca, 2012). The sensor detects stagnant water, generally all flat surfaces, with a low backscatter intensity due to the specular reflection of the incident SAR rays (Richards et al., 1987). This processing of SAR images allow to assess (a) the extension of the flooding and (b) the depth of flooding if an accurate model of digital elevation is available (Cian, Marconcini, & Ceccato, 2018). Figure 1a–c shows the satellite images of the days 28, 30 and August 31, 2017, respectively.

TABLE 2 Data sources

Data	Sources
Precipitation satellite data (TRMM and GPM)	www.giovanni.gsfc.nasa.gov
CHIRPS	http://iridl.ldeo.columbia.edu/SOURCES/UCSB/CHIRPS/.v2p0/daily-improved/global/.0p05/.prcp/
NCEP-CPC	http://iridl.ldeo.columbia.edu/SOURCES/NOAA/NCEP/CPC/Merged_Analysis/.pentad/
NCEP-GOB	http://iridl.ldeo.columbia.edu/SOURCES/NOAA/NCEP/CPC/GOB/.V0px/.daily/.REALTIME/.prcp/

Abbreviations: CHIRPS, rainfall estimates from rain gauge and satellite observations; TRMM, tropical rainfall measuring mission; GPM, global precipitation measurements; NCEP-CPC, National Center for Environmental Prediction—Climate Prediction Center; NCEP-GOB, National Center for Environmental Prediction—Global observation.

2.4 | Social media data

The social media markers used in the study were provided by the Evolution of the Emergency Copernicus database (E2mC) owned by Copernicus (Scalia, 2017). The markers obtained from this research project refer to the same dates as the satellite images described above. This service is mainly based on the integration of information derived from remote sensing, spatial analysis algorithms, social media and crowdsourcing. All these data are collected by remote digital volunteers and local journalists. For a detailed description of how the posts are extracted, geolocated and made available, see Havas et al., 2017. In Figure 2a the spatial distribution of the markers obtained for the days of the extreme event are shown. An example of photograph used in the analysis is shown in Figure 2b.

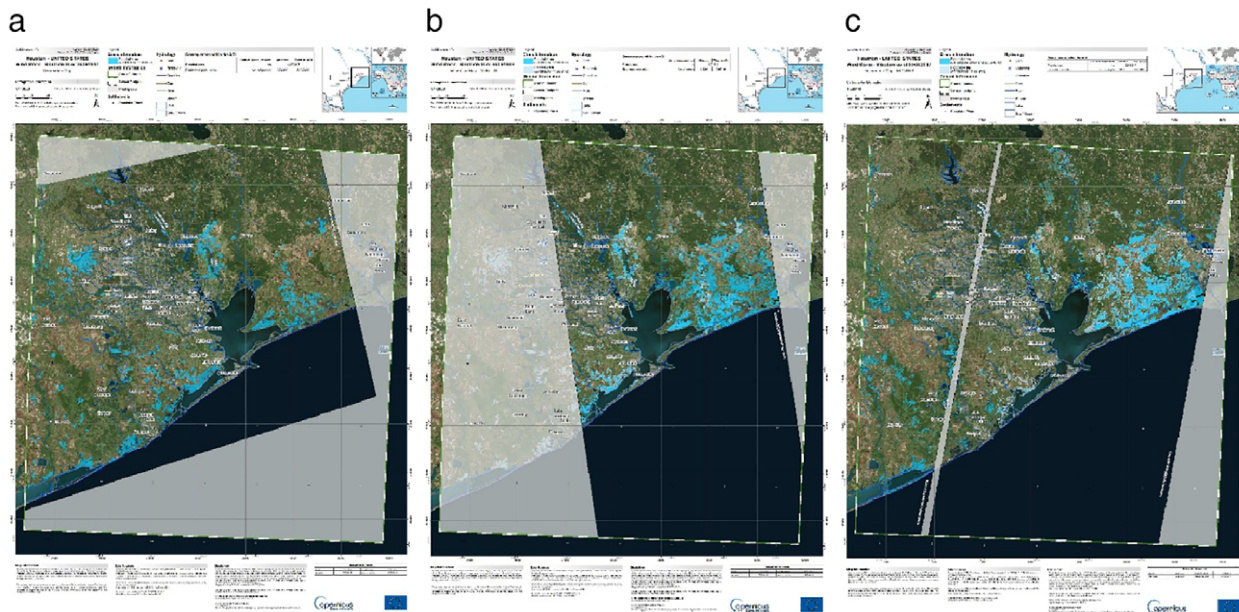


FIGURE 1 Flooding maps by satellite images during Harvey Hurricane of (a) August 28, 2017, (b) August 30, 2017, and (c) August 31, 2017

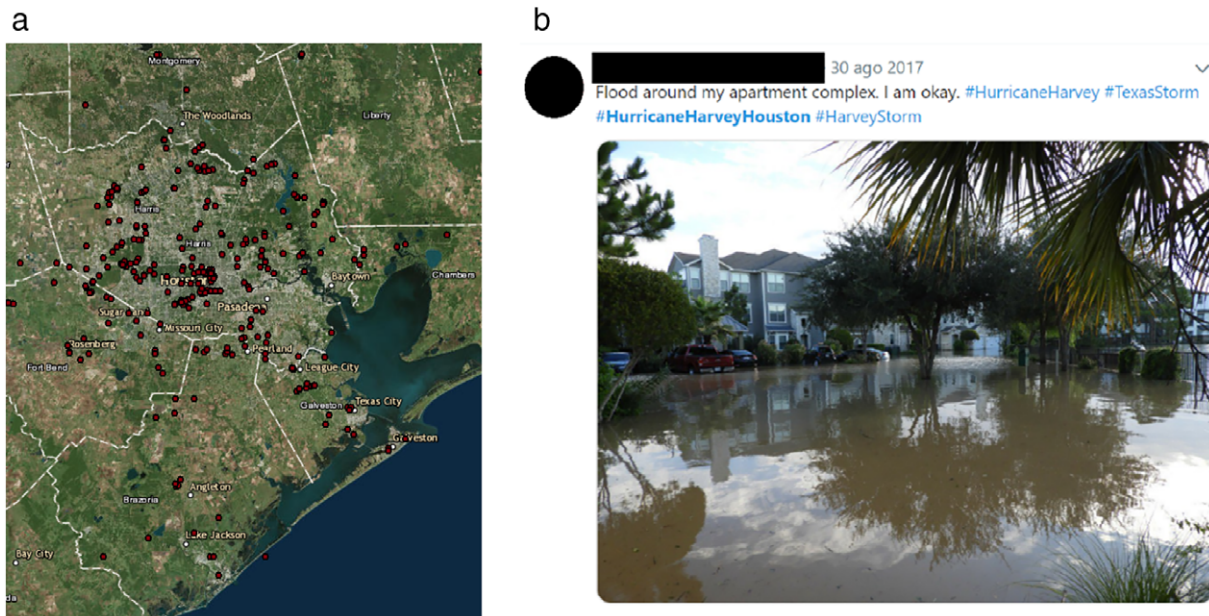


FIGURE 2 (a) Location of social media marker in Houston and (b) example of photo used for the hydraulic model validation (obtained from E2mC)

2.5 | Hydraulic modelling

The 2D hydraulic model, the USACE Hydrologic Engineering Center's River Analysis System (HEC-RAS 5.0.7) was used. Such Hydraulic Numerical Models is a public domain software that meets the minimum requirements of National Flood Insurance Program as required by FEMA (<https://www.fema.gov/hydraulic-numerical-models-meeting-minimum-requirement-national-flood-insurance-program>). Recent FEMA report (<https://www.fema.gov/media-library-data/1561469561757-6fed6a4fd077673f684920b9ad5a0e53/RapidResponseFloodModelingFinalReport.pdf>) shows that the model produces results with higher precision (*SD*) and predictive value (correlation) than other models.

The code, whose details can be found in HEC-RAS, River Analysis System Hydraulic Reference Manual, solves either the 2D shallow water equations (with optional momentum additions for turbulence and Coriolis effects) or the 2D Diffusion Wave equations. In the case study, full momentum equations were used. The equations in HEC-RAS are solved with an implicit finite volume algorithm. This algorithm allows the use of a structured or unstructured computational mesh. Local thickening of computational mesh can be applied by break lines, added along levees, buildings, roads, and in abrupt slope change.

In HEC-RAS 2D modelling the mesh size can be arbitrarily chosen. Generally, to limit the computational time, especially for large integration domains,

computational mesh sizes coarser than the spatial DEM resolution are used. This would result in a rough representation of the domain geometry in particular in building areas or in presence of abrupt ground level changes. However, to take into account the details of the underlying terrain, at least at the DEM resolution, the subgrid approach proposed by Casulli (2009) is integrated in the algorithm.

The approach taken is to calculate volume and mass/momentum fluxes through the cell faces at the coarser scale by the modification of the continuity and momentum equations, expressed in integral form, to account the variability of the ground level and the presence of obstructions as represented at finer DEM scale. For this purpose, using the DEM, a relationship describing the variation of the wet volume and area of the faces as a function of water elevation, is first calculated for each cell. With this approach it is possible to exploit the high topographic information resolution obtainable from DEM and, at the same time, to use calculation cells with a size coarser than the resolution of the input data.

The HEC-RAS code simulates wet and dry conditions and allows the direct application of the precipitation. Neither spatial variation of precipitation nor losses and infiltration are currently able to be used within HEC-RAS. In cases in which pluvial contributions and their spatial and temporal variability play a determinant role in producing flooding these limitations could represent a serious drawback.

3 | CASE STUDY

For the case study, the domain of integration as delimited by the watershed ridge shown in Figure 3 was selected. In this way there was no surface runoff from external regions, and the flooding within the domain was due only to rainfall and/or to storm surge along the coast. Thus, the calculation of flow entering in the domain by rainfall-runoff hydrological models, which requires a preliminary very complex model parameter identification, was avoided. A DEM with a 5 m resolution was obtained from the USGS (United States Geological Survey, link: <https://viewer.nationalmap.gov/basic/>). Due to the very large size of the domain, a nominal grid resolution (250×250 m) was selected and the computational mesh was constructed by the HEC-RAS tools. In the zones where a higher resolution was required, break lines were introduced to obtain a resolution up to 5 m.

The land cover map extracted from Copernicus images related to the period of the flood (August 2017) is shown in Figure 3. Most of the territory within the domain boundaries is covered by forest or urban areas. The values of Manning resistance coefficient were defined for each

point of integration in the domain as a function of the Land Use classification, according to Table 3.

In the present case study, due to the exceptional rainfall event, precipitation was rather spatially uniform. Therefore a precipitation spatial average over the integration domain was applied. Furthermore, the rainfall amount was so exceptionally high that the soils, independently from their nature, were completely saturated in a short time. This is seen in Figure 4 where the temporal variation of the instantaneous runoff coefficient (Equation (1)) is shown as function of the precipitation trend. The figure refers to typical values of saturation coefficient k (Table 1) that are characteristic of different land cover types. To further confirm the high level of soil saturation, NASA analysed the soil moisture in south-eastern Texas before and after Harvey landing using data from NASA's Soil Moisture Active Passive (SMAP) satellite. SMAP observations from August 2017 21st and 22nd showed that soil surface conditions were already very wet a few days before the hurricane made landfall, with 20–40% moisture levels (<https://phys.org/news/2017-08-nasa-harvey-saturated-areas-texas.html>).

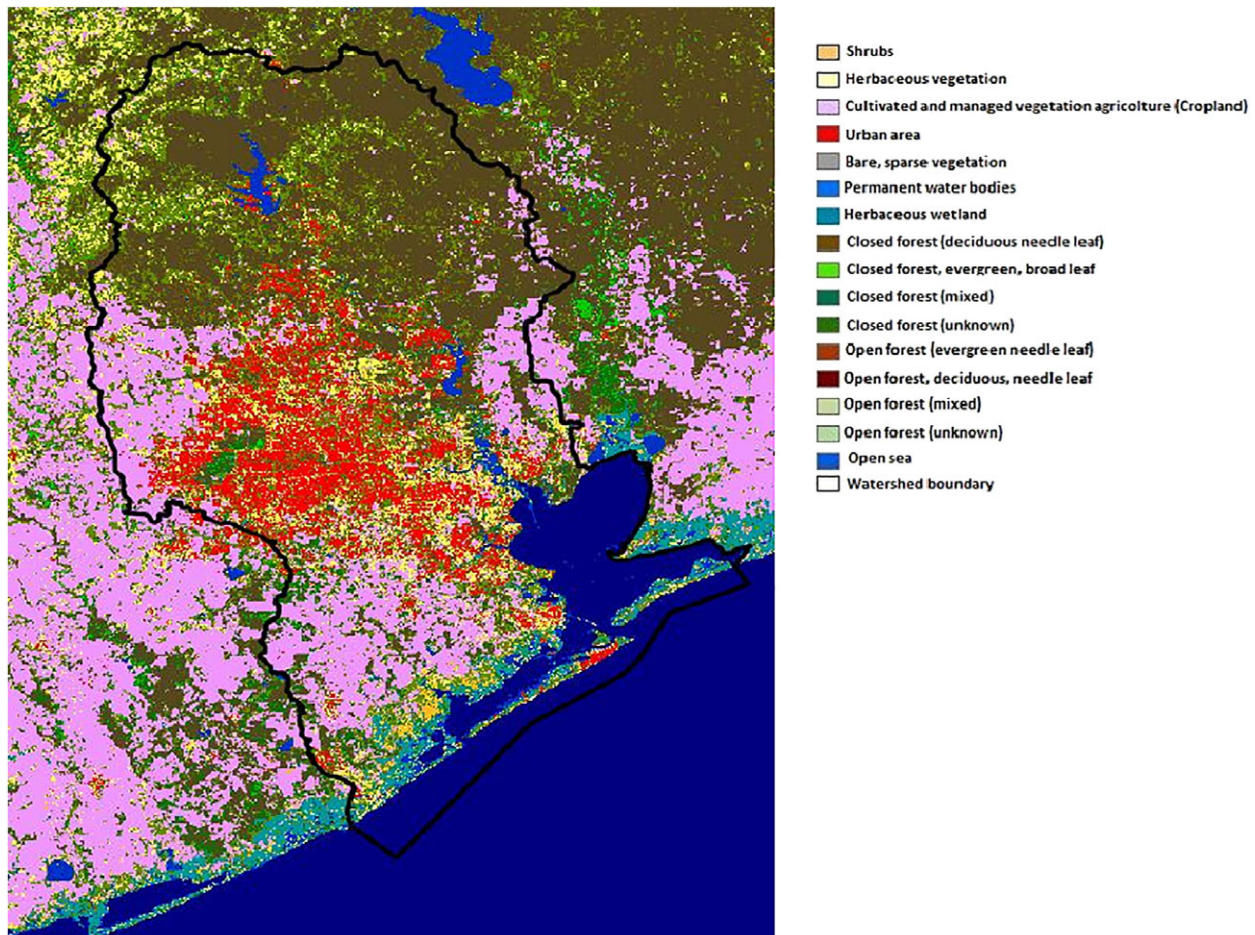


FIGURE 3 Land cover by supervised classification algorithm on Copernicus images

The sea level trend, due to the storm surge, and recorded during the extreme event along the coastal, was applied as boundary condition (www.u-surge.net/hurricane-harvey.html).

3.1 | Model calibration

First, several simulations were carried out for different values of the saturation factor k appearing in Equation (1). Then for each model simulation, the fitting index

TABLE 3 Spatial variability roughness used in the hydraulic model

Land cover type	Default manning valued ($\text{m}^{1/3} \text{s}^{-1}$)
Natural vegetation, shrubs and cropland	0.04
Herbaceous vegetation	0.045
Developed (urban area)	0.25
Main channel	0.022
Barren land rock/sand/clay	0.04
Permanent water bodies	0.035
Mixed and evergreen forest	0.08
Bare, sparse vegetation	0.02
Herbaceous wetland	0.16
Sea	0.03

$I(k)$, defined by Equation (2), was calculated. Simulated flooding areas A_{sim} belonging to urban and forest land cover types were excluded from the calculations of $I(k)$.

Figure 5 shows the flooding map for August 28th at 11 a.m. – obtained from the hydraulic simulation for $k = 0.004 \text{ mm}^{-1}$, at which corresponds the highest fitting index value.

Comparing the inundation map in Figure 5, with that obtained by satellite image (shown at the left side of Figure 6), clearly shows how in urban and forest land cover areas the flooding is not recognised by satellite, despite the evidence in Figure 5 of large inundated areas.

However, as Figure 6 shows (right side), in rural areas, the location and extent of flooding areas – simulated and detected by satellite images – is satisfactory. Values of the fitting index ranges from 0.60 to 0.80 were obtained for the rural flooding areas selected.

To confirm the goodness of the calibration procedure, in Figure 7 (right side) the simulated and measured time series of free surface level in correspondence of some hydrometric gauges (Figure 7 left side), homogeneously distributed in the areas of interest, are compared. As shown in Figure 7 (right side) the simulated free surface trends at the different locations satisfactorily fits the actual trend of observed values.

Furthermore, the timing of the simulated and observed bank overflows in different cross sections of bayous passing through the urban Houston area, was

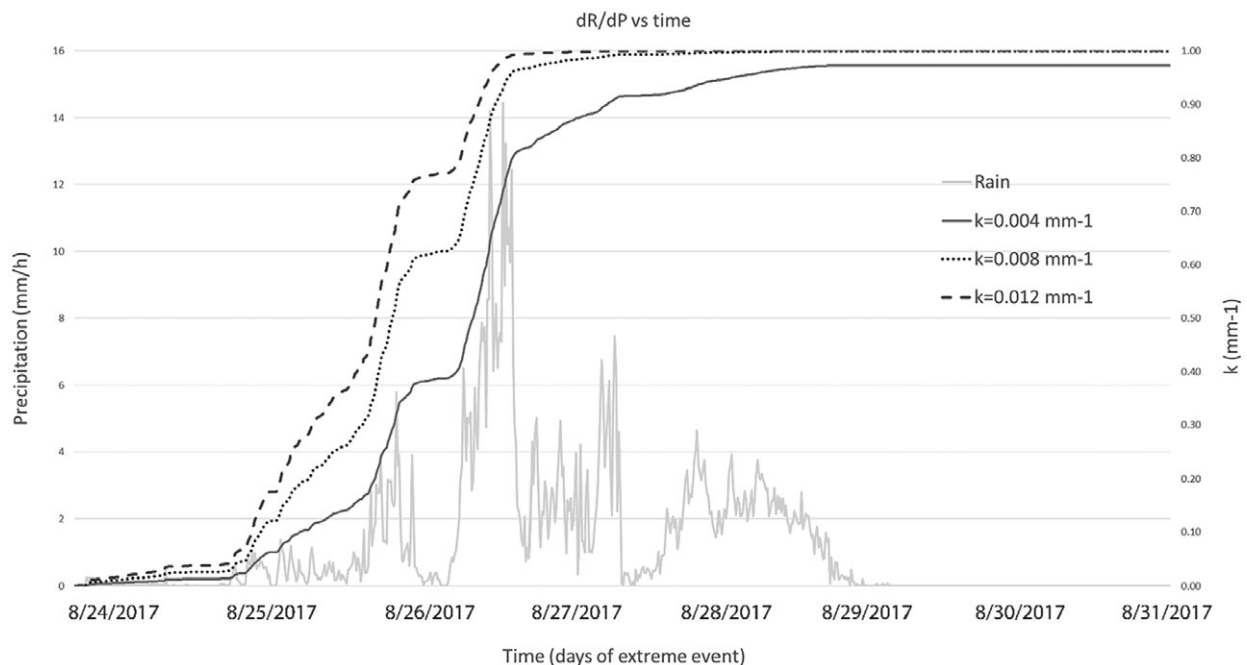


FIGURE 4 Rainfall amount (right) and runoff rate dR/dP for different values of k (left)

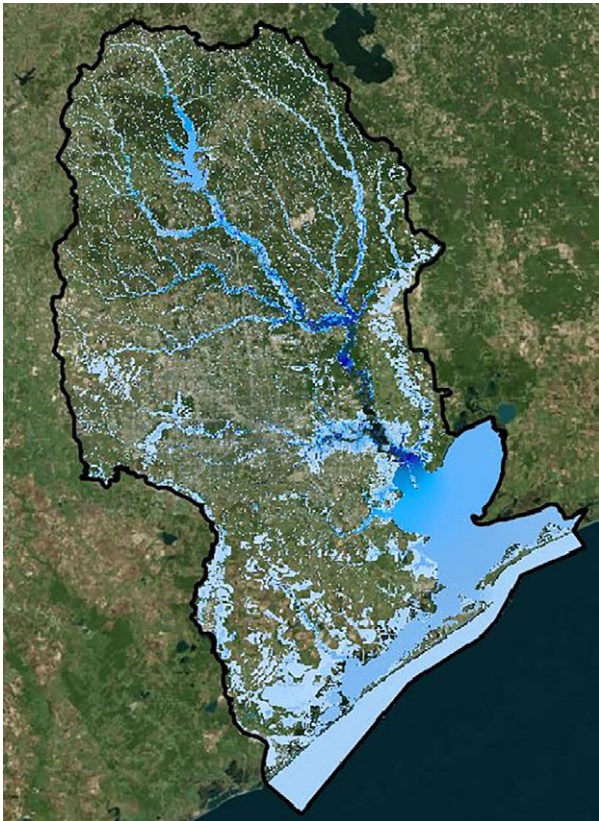


FIGURE 5 Flooding map obtained from hydraulic modelling ($k = 0.004 \text{ mm}^{-1}$)

compared. The network of the alert stations presents in the Houston area and owned by the HCFCD was used. In the Harris maps (shown in the left side of Figure 8), the red symbols indicate the locations where the water level exceeds the top of the bank, the yellow where the level is near the top of the bank and the green when the water flows inside the bank. All the maps are referred to the same hour, for all the days considered, at 11.30 a.m. The comparison, shown in Figure 8, demonstrates that the hydraulic model simulation followed the temporal trend of the floods during the days of the extreme rainfall event.

3.2 | Model validation by social media markers

The comparison between the simulated water depths with those estimated by the photographs at the same location and time, adds an additional element of judgement, in particular in urban areas where satellite is not able to recognise the flooding (Figure 9).

In Table 4, the water depth estimated by social marker and simulated at the locations of Figure 9 are shown.

The comparison of Table 3 demonstrates the proposed approach was satisfactory for the quantification of flow

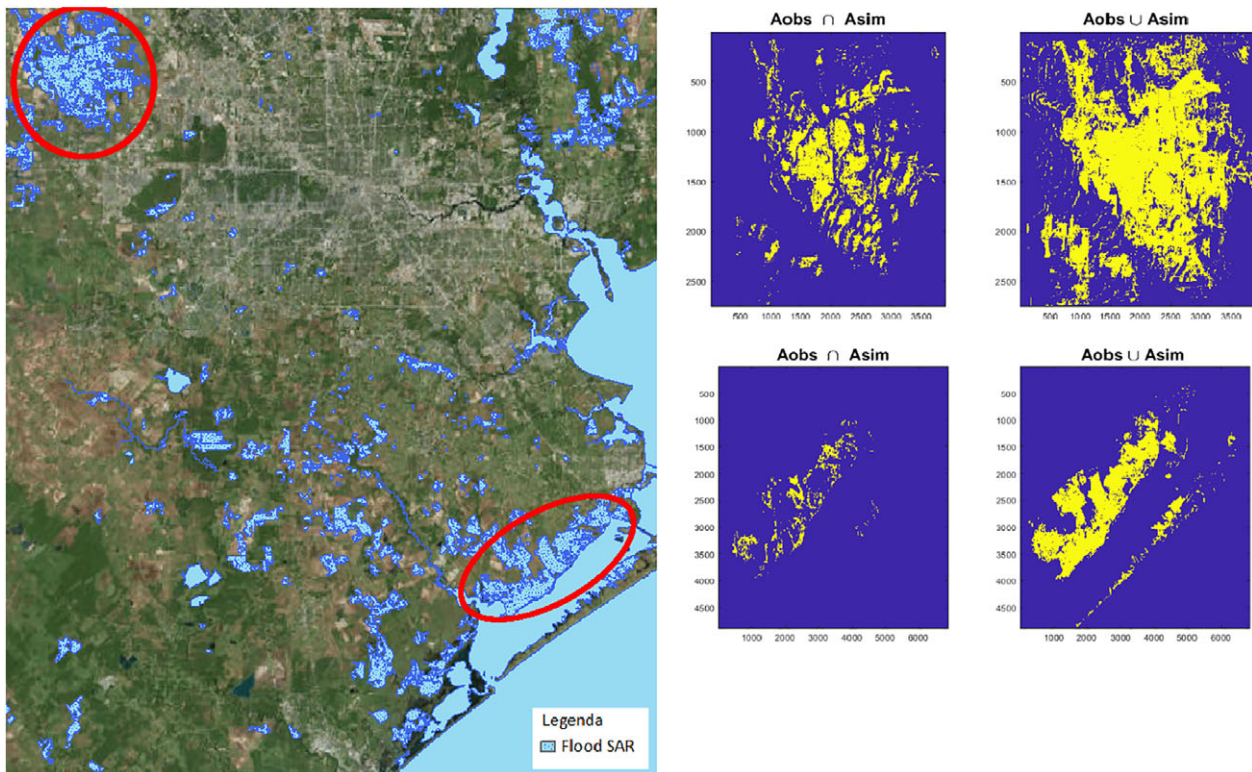


FIGURE 6 Correspondence between the flooding areas obtained by hydraulic simulation and synthetic-aperture radar satellite

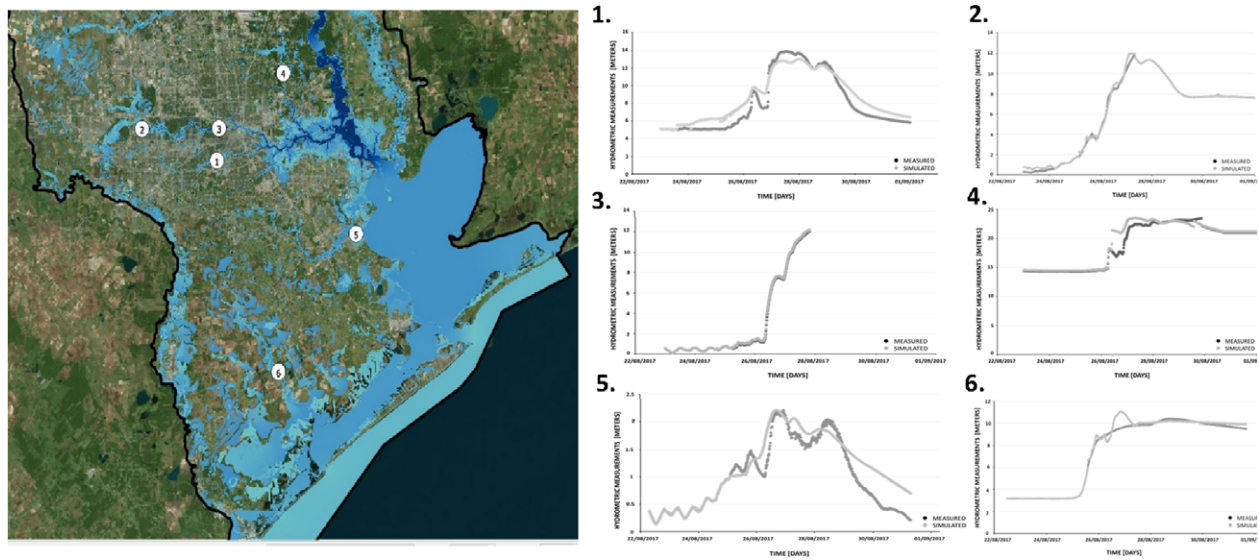


FIGURE 7 Location of measurement stations of the levels considered and hydrometric levels detected during the extreme event

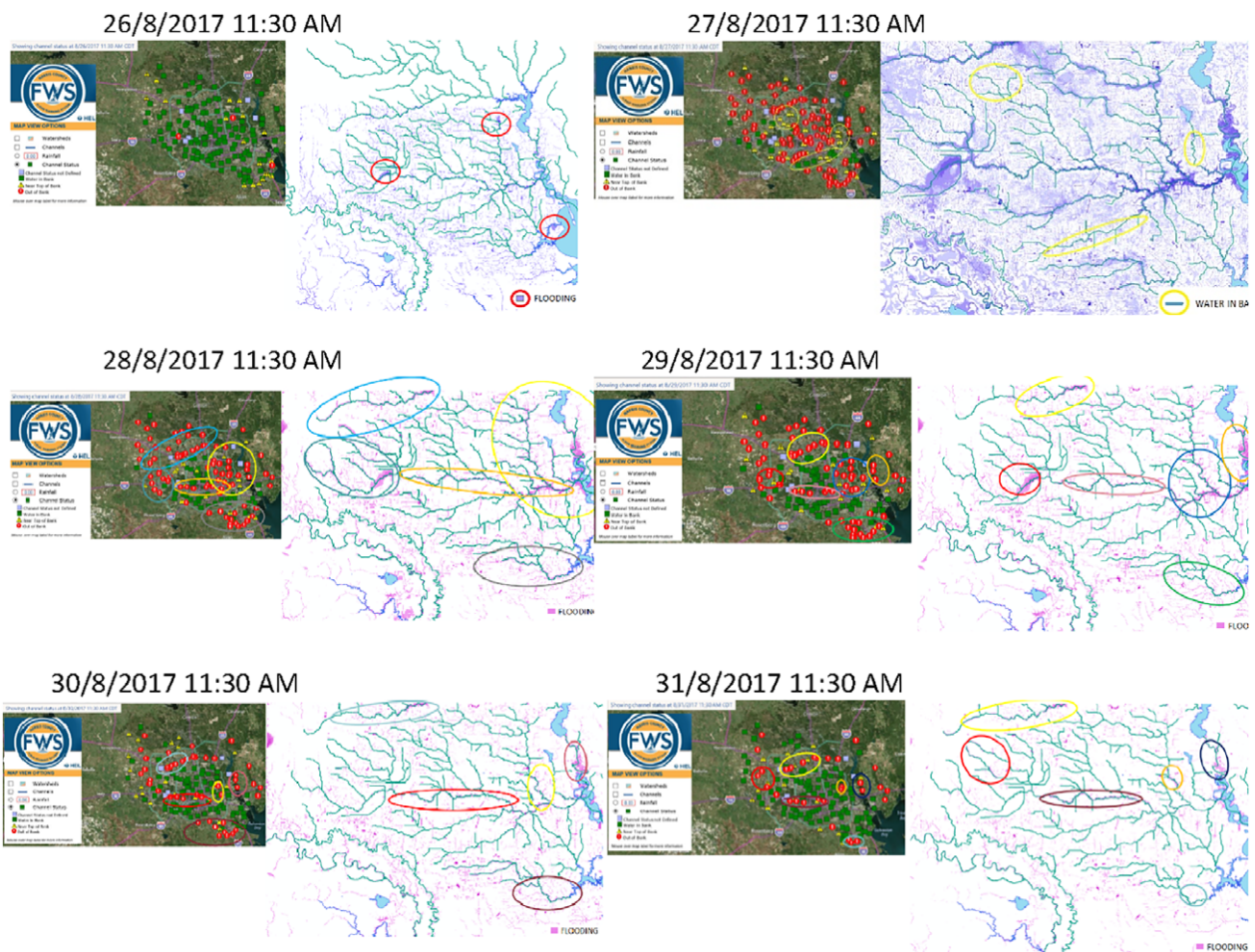


FIGURE 8 Temporal trend of the floods in Houston during Hurricane Harvey from 26/08 to 31/08. Red symbols indicate the locations where the water level exceeds the top of the bank, the yellow where the level is near the top of the bank and the green when the water flows inside the bank



FIGURE 9 Social media marker referred at the same day of the flooding maps (August 28, 2017) used for the result validation

TABLE 4 Comparison between water depth (m) estimated by social marker and simulated by hydraulic model

Identification colour	Depth by hydraulic modelling (m)	Depth estimated by social media marker (m)
White	2	2 ± 0.10
Purple	0.4	0.5 ± 0.10
Pink	0.35	0.3 ± 0.10
Red	0.5	0.5 ± 0.10
Violet	2.7	2.5 ± 0.10
Light green	0.4	0.5 ± 0.10
Light yellow	Bayou 7 other 1.5	Bayou 5 ± 0.1 other 1 ± 0.1
Dark green	1.8	1.5 ± 0.10
Orange	0.56	0.5 ± 0.10
Yellow	0.8	1 ± 0.10

depth and velocity, as well as inundation timing, in urban areas where such flow characteristics are more challenging to detect, even given uncertainties in deducing the water depth from the photographs.

3.3 | Further insights from the study case

As the validation of the social markers has shown, we were able to obtain an accurate flooding map of the event, even in urban areas where satellite data fail to provide information. This result was also due to: (a) the availability of well spatially distributed ground-based rainfall data; (b) the local thickening of the calculation mesh by break lines, to take into account the complex geometries present in the study area such as buildings, sudden slope changes, presence of levees, etc. However, the application of the break line required a very tedious and long work for the calculation grid construction.

The above observations suggested an exploration of the two following issues:

1. In absence of rain gauges in the study areas, could remote sensing provide the temporal and spatial distribution of precipitation to be effectively used as hydraulic model inputs?
2. In order to reduce the computation time, what are the potential inaccuracies of the hydraulic model used (HEC-RAS 5.0.7) in simulating flows in urban areas if

we integrate 2D motion equations on a coarser grid, without using break lines?

3.4 | Comparison between measured rainfall amount by rainfall gauges and remote sensing

In order to provide an answer at the first issue, we first compared the rainfall temporal and spatial distribution from ground-based station measurements with TRMM satellite precipitation data recorded during the Harvey Hurricane. Then, we compared the heavy daily rainfall amount – identified by 95th, 99, and 99.9 percentile – of a longer time series of wet days obtained from different sources of remote sensing precipitation datasets, and from an ensemble of rain gauges in a more restricted area of Houston.

Figure 10 shows the time series of spatially averaged precipitation from the ensemble of ground measurement stations (light grey) and from TRMM (dark grey). An evident underestimation of both peak and volume of rainfall amount obtained by satellite can be observed.

For the analysis of heavy rainfall, a more restricted area of Houston ($0.1^\circ \times 0.1^\circ$) was taken into account. The rain gauge and remote sensing precipitation time series, from the year 2003 to the year 2017 were used, with the exception of the GPM (Global Precipitation Measurement), which covers the shorter period 2014–2017. To select the remote sensing dataset we referred to the papers of Sun

et al., 2018, Tan & Santo, 2018, Omranian & Sharif, 2018 and Beck et al., 2017. The comparison between the heavy rainfall from ground-based and remote sensing records was based on the following error index:

$$CV(RMSE) = \frac{\sqrt{\sum_{i=1}^N \left[\frac{(M_i - S_i)^2}{N} \right]}}{\frac{1}{N} \sum_{i=1}^N M_i} \quad (3)$$

where M_i and S_i are respectively ground based and remote sensing data at instance i , and N is the total number of data.

CV(RMSE) (cross-validated root mean square error) represents the coefficient of variation of the average standard deviation, that is, the ratio between the average square deviation of a certain period and the mean value of the data measured in the same period (Beck et al., 2017; Royapoor & Roskilly, 2015). Table 5 shows the datasets used and corresponding CVRMS errors.

From Table 5 we can observe how the biases are rather large, resulting in each case in an underestimation of the effective heavy rainfall amount. The best dataset seems to be the GPM, but in this case bias is also large. This analysis suggests that the use, as input for hydraulic simulations, of precipitation intensity measured by remote sensing datasets should be made carefully, taking into account the existence of such bias. It also suggests that more research efforts should be made to overcome this drawback.

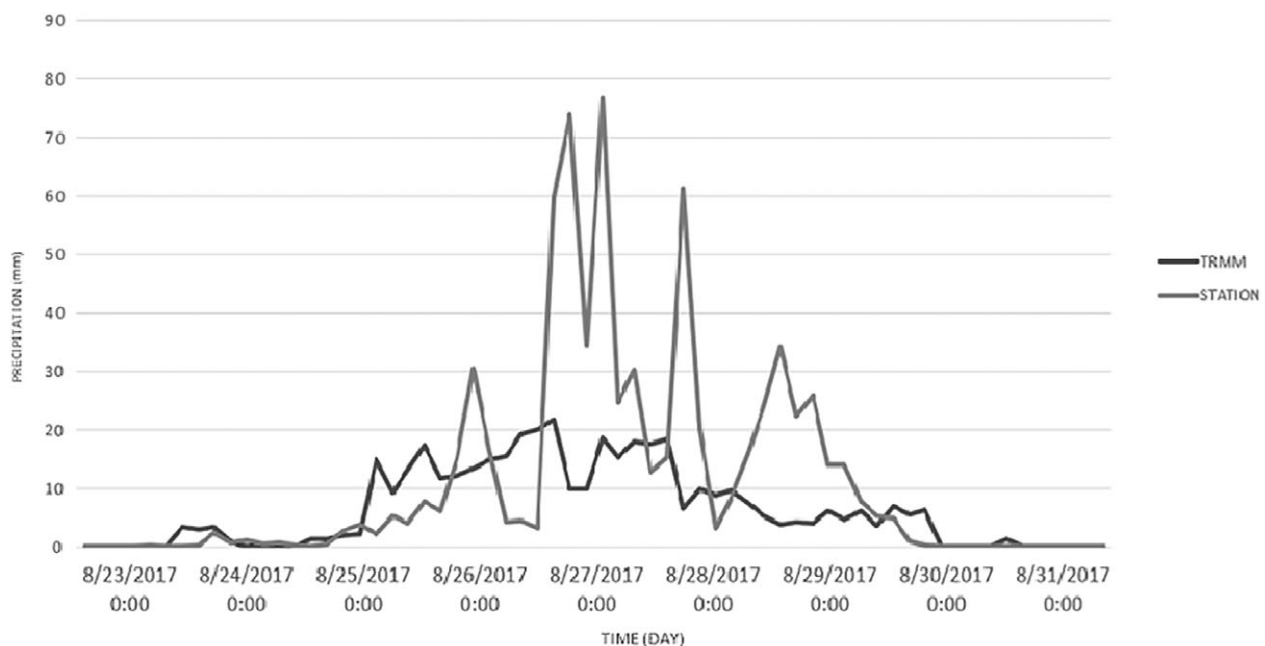


FIGURE 10 Comparison between the rainfall amount trend recorded by rain-gauges and that from satellite (tropical rainfall measuring mission) during the Harvey Hurricane

3.5 | The potential inaccuracies of the hydraulic model (HEC-RAS 5.0.3) in simulating flows in urban areas

Accurate model hydraulic simulation would require a computational mesh size with the same DEM resolution. However, for large integration domain, this implies high

TABLE 5 Values of CV(RMSE) referred to 95, 99, and 99.9 percentile

Data set	95 percentile	99 percentile	99.9 percentile
TRMM-3B42	0.78	0.60	0.41
CHIRPS	0.79	0.72	0.76
NCEP-CPC	0.99	0.63	0.54
NCEP-GOB	0.89	0.81	0.36
GPM	0.61	0.58	0.22

Abbreviations: CV(RMSE) Cross-validated root mean square error; CHIRPS, rainfall estimates from rain gauge and satellite observations; TRMM, tropical rainfall measuring mission; GPM, global precipitation measurements; NCEP-CPC, National Center for Environmental Prediction—Climate Prediction Center; NCEP-GOB, National Center for Environmental Prediction—Global observation.

computational times, especially in the case of high-resolution DEM (i.e., Lidar data, etc.). Thus, we explore how the model accuracy is affected by the use of a coarser mesh, in which the flow motion frictions due to the presence of buildings and other urban structures are solved by the HEC-RAS subgrid approach.

A number of simulations on a structured computational grid with mesh size: 5×5 m; 10×10 m; 25×25 m; 50×50 m; 100×100 m; 250×250 m, and 500×500 m were thus performed. The simulations refer to an integration domain which covers an urban portion of Houston city (see Figure 11).

The boundary conditions were applied as: (a) at the upstream boundary of the domain the flow rates were imposed in according to a simple hydrograph in which the flow rate increases linearly in 15 min from zero to $20 \text{ m}^3/\text{s}$, beyond that flow rate is maintained constant; (b) at downstream boundary normal flow condition was applied. The simulation period was long enough to allow steady flow conditions to be established.

The following errors were defined to estimate the effect of the different mesh sizes on the simulated depth and velocity fields:

$$h_{err} = \frac{h_{5 \times 5} - h_{DIM > 5 \times 5}}{h_{5 \times 5}} \quad (4)$$

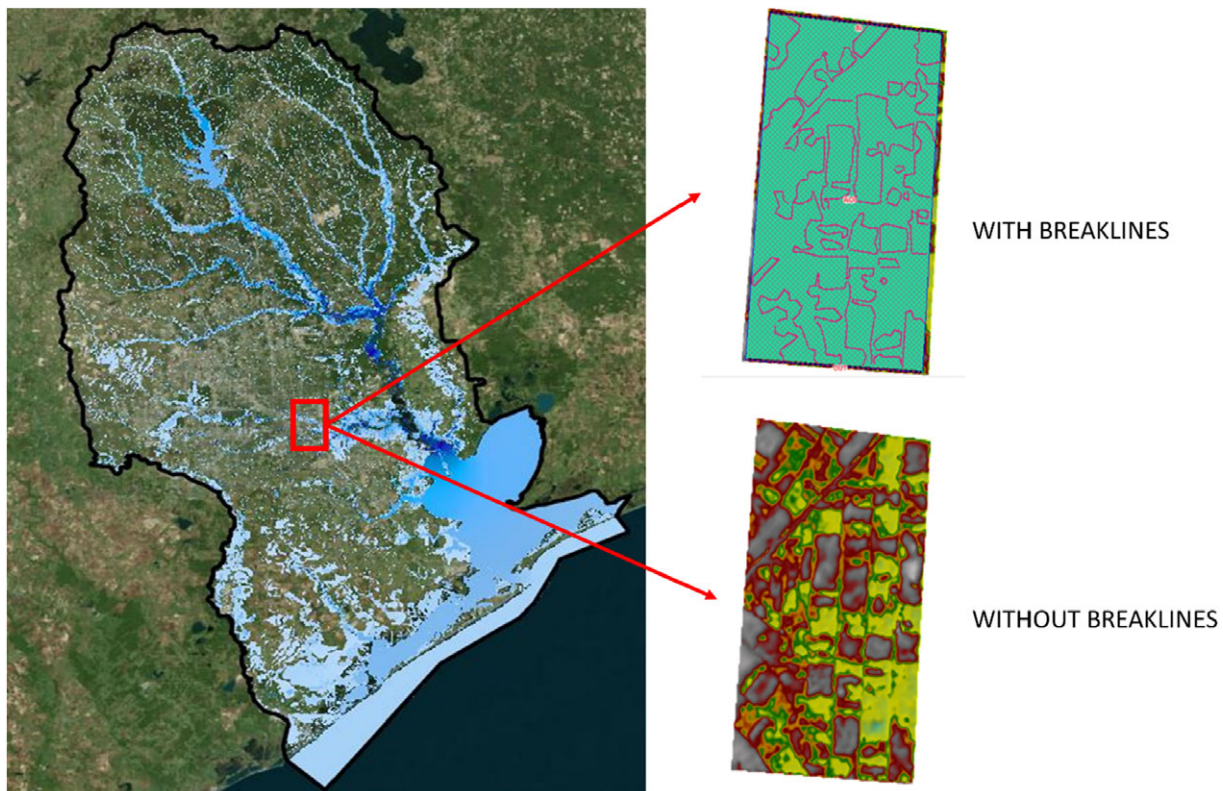
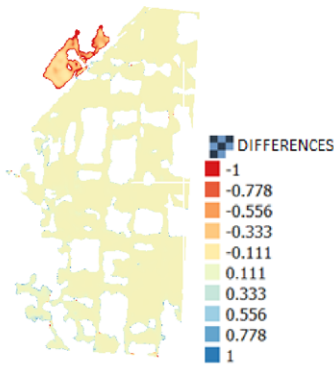
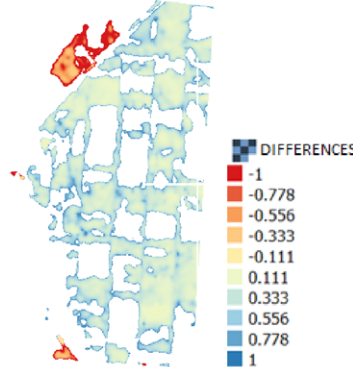


FIGURE 11 Area used for the subgrid test (the break lines are visible as pink lines)

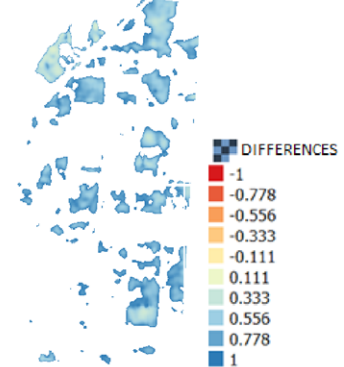
Depth 5x5 vs 10x10



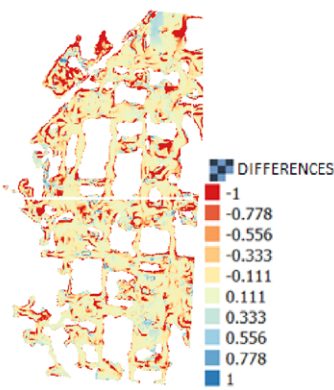
Depth 5x5 vs 100x100



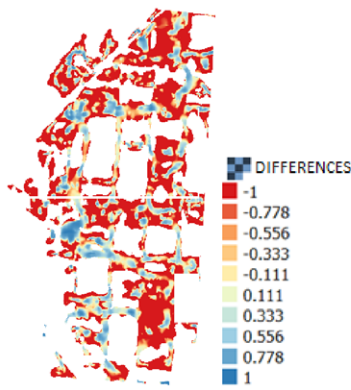
Depth 5x5 vs 500x500



Velocity 5x5 vs 10x10



Velocity 5x5 vs 100x100



Velocity 5x5 vs 500x500

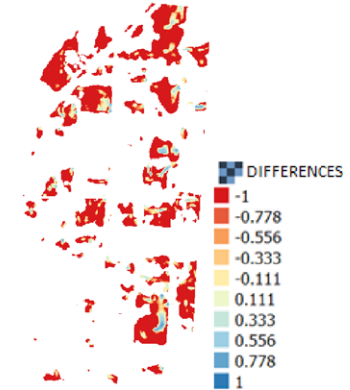


FIGURE 12 Hydraulic simulation results for the depth and velocity at the mesh size 5×5 vs 10×10 , 100×100 and 500×500

TABLE 6 Ratio between flooding area from model simulations on coarser mesh (10×10 , 25×25 , 50×50 , 100×100 , 250×250 , 500×500) and reference flooding area (mesh size 5×5 m)

	10×10 vs 5×5	25×25 vs 5×5	50×50 vs 5×5	100×100 vs 5×5	250×250 vs 5×5	500×500 vs 5×5
A ref (5×5)/A subgrid	0.958066373	0.87686	0.7914	0.66211	0.2649137	0.14976

$$v_{err} = \frac{v_{5 \times 5} - v_{DIM > 5 \times 5}}{v_{5 \times 5}} \quad (5)$$

In Figure 12 the errors obtained by Equations (4) and (5) are shown for mesh sizes of 10×10 , 100×100 , and 500×500 m, respectively.

Figure 12 shows the increase of the errors with mesh size increasing. Such errors are significantly greater for flow velocity than for flow depth.

Table 6 shows the ratios between the extensions of the flooding obtained using the different mesh sizes and the 5×5 m ones. As the size of the calculation cells increases, the flooding extension significantly decreases (see Figure 12) with a notable loss of accuracy.

4 | CONCLUSIONS

In the paper we applied an approach to post-event flooding maps by integrating satellite images, hydraulic model simulations and social markers. Inundation areas detected by satellite images was used to calibrate the hydraulic numerical model, whose simulations were validated by information extracted by the social markers. Few attempts have been made in the past to integrate these different tools, and we believe that this study could be a stimulus.

The application to the inundation of Houston area by Hurricane Harvey showed that this approach allows a credible reconstruction of the main flooding characteristics -

flow depth and velocity, as well as flooding timing, which are relevant information for a correct post-event damage evaluation or to plan future flood defence systems. Specifically, the approach has been shown to be reliable in flooding reconstruction in urban areas where the detection of inundate areas by satellite images is still challenging. In fact, it has been shown that in the presence of buildings, roads, shadows, rough terrain, dense vegetation, and detection methods based on SAR fail to recognise flooding areas. Hydraulic model simulations allow to overcome such limitation, but in order to reduce the computational time by using mesh with a resolution coarser than the DEM resolution, we need to use a sub-grid approach, which could be a further source of inaccuracies. In this context model validation in the urban areas by social markers assures on the reliability of the flooding reconstruction.

However, the application to the case study has highlighted some drawbacks of each component method. First, detection techniques based on satellite images suffer of the difficulty to extract coherent information of flooding in urban areas being the satellite signal affected by complex backscattering mechanisms. Indeed such techniques mainly focus on detecting flooding in rural or suburban areas. Furthermore, the false positives and negatives that frequently appear in the images need to be addressed through a subjective evaluation of the operators with consequent loss of accuracy.

Our comparison with rainfall amount time series recorded by rain-gauge shows that heavy rainfall amount recorded by remote sensing are affected by significant underestimation. Such bias should be significantly reduced, for satellite-based rainfall to be a viable source of information. However, new generations of satellites, with higher temporal and spatial resolution, should allow the development of new methods and tools for flooding detection to overcome the above listed drawbacks, especially in urban areas, providing more reliable flooding data for calibration of hydraulic numerical model as well as more reliable rainfall amount measurements, especially for heavy precipitation for providing model input.

The inability in HEC-RAS to use spatially varying precipitation input, as well as, the impossibility to take into account losses and infiltration in dependence of soil and/or land cover characteristics, can be a serious impediment to obtain accurate simulations. In the case study, due to the exceptional Harvey precipitation event, these limitations have not affected the reliability of the result. However, in other situations they could seriously affect them. Extensions to remedy this, would avoid the need to switch to a different model. The case study shows that HEC-RAS is effective for simulating flooding in urban areas in domains that are not particularly large, where the mesh resolution is of the same order of magnitude of

the DEM resolution. However, for large regions, in order to maintain the same accuracy, break lines have to be applied to fit more complex geometry elements like building, levees, etc. The consequence of such application is a significant increase of computational times. Alternatively a coarser mesh could be used together with previously described subgrid approach. The analysis conducted for the case study has unfortunately shown that increasing the computational grid size the results are affected by large errors for both flow velocity and depth. The consequence is a considerable loss of information about flooding extension and timing. The errors grow with the increase of the grid size. For water depth, errors are lower than for flow velocity but still significant. This fact suggests that more efforts should be directed towards improving subgrid models, particularly for simulating free surface flows in urban areas. Alternatively, other strategies should be explored in order to reduce computation times for high resolution simulation.

Social markers have shown to be very effective for verify the goodness of the reconstruction by model of the flooding in the urban areas of Houston, since in the case study, they have provided a lot of very well-defined spatial and temporal data about the depth of the flooding. Since the demonstrated usefulness of social markers, planning a rational distribution on the territory of cameras or a citizen awareness about the opportunity to share information about the evolution of flooding event would be opportune. These latter would reduce the tedious extraction of data from social markers which often require the need also of subjective analysis.

ACKNOWLEDGEMENT

The authors are thankful to the anonymous reviewers and associate editor for their helpful comments to revise the paper. The authors are greatly also acknowledged to Prof. Pietro Ceccato for his useful suggestions.

DATA AVAILABILITY STATEMENT

Data sharing is not applicable to this article as no new data were created or analyzed in this study.

ORCID

Vincenzo Scotti  <https://orcid.org/0000-0001-5052-5487>

REFERENCES

- Alcrudo, F., & Garcia-Navarro, P. (1993). A high-resolution Godunov type scheme in finite volumes for the 2D shallow water equations. *International Journal for Numerical Methods in Fluids*, 16, 489–505.
- Anastasiou, K., & Chan, C. T. (1997). Solution of the 2D shallow water equations using the finite volume method on unstructured triangular meshes. *International Journal for Numerical Methods in Fluids*, 24, 1225–1245.

- Auynirundronkool, K., Chen, N., Peng, C., Yang, C., Gong, J., & Silapathong, C. (2012). Flood detection and mapping of the Thailand central plain using RADARSAT and MODIS under a sensor web environment. *International Journal of Applied Earth Observation and Geoinformation*, 14(1), 245–255.
- Bales, J. D., & Wagner, C. R. (2009). Sources of uncertainty in flood inundation maps. *Journal of Flood Risk Management*, 2, 137–147.
- Balzano, A. (1998). Evaluation of methods for numerical simulation of wetting and drying in shallow water flow models. *Coastal Engineering*, 34, 83–107. [http://dx.doi.org/10.1016/S0378-3839\(98\)00015-5](http://dx.doi.org/10.1016/S0378-3839(98)00015-5).
- Bates, P., & Hervouet, J. (1999). A new method for moving-boundary hydrodynamic problems in shallow water. *Proceedings of the Royal Society of London. Series A*, 455, 3107–3128 [10.1098/rspa.1999.0442](https://doi.org/10.1098/rspa.1999.0442).
- Beck, H. E., Vergopolan, N., Pan, M., Levizzani, V., van Dijk, A. I., Weedon, G. P., ... Wood, E. F. (2017). Global-scale evaluation of 22 precipitation datasets using gauge observations and hydrological modeling. *Hydrology and Earth System Sciences*, 21(12), 6201–6217.
- Brivio, P. A., Colombo, R., Maggi, M., & Tomasoni, R. (2002). Integration of remote sensing data and GIS for accurate mapping of flooded areas. *International Journal of Remote Sensing*, 23(3), 429–441.
- Carincotte, C., Derrode, S., & Bourennane, S. (2006). Unsupervised change detection on SAR images using fuzzy hidden Markov chains. *IEEE Transactions on Geoscience and Remote Sensing*, 44(2), 432–441.
- Casas, A., Lane, S., Yu, D., & Benito, G. (2010). A method for parameterising roughness and topographic sub-grid scale effects in hydraulic modelling from Li-DAR data. *Hydrology and Earth System Sciences*, 14, 1567–1579. <http://dx.doi.org/10.5194/hess-14-1567-2010>.
- Casulli, V. (2009). A high-resolution wetting and drying algorithm for free-surface hydrodynamics. *International Journal for Numerical Methods in Fluids*, 60(4), 391–408.
- Chang, N. B., & Guo, D. H. (2006). Urban flash flood monitoring, mapping and forecasting via a tailored sensor network system. In *2006 IEEE International Conference on Networking, Sensing and Control* (pp. 757–761).
- Chini, M., Pulvirenti, L., & Pierdicca, N. (2012). Analysis and interpretation of the COSMO-SkyMed observations of the 2011 Japan tsunami. *IEEE Geoscience and Remote Sensing Letters*, 9(3), 467–471.
- Chini, M., Papastergios, A., Pulvirenti, L., Pierdicca, N., Matgen, P., & Parcharidis, I. (2016). SAR coherence and polarimetric information for improving flood mapping. In *2016 IEEE International Geoscience and Remote Sensing Symposium (IGARSS)* (pp. 7577–7580).
- Cian, F., Marconcini, M., & Ceccato, P. (2018). Normalized difference flood index for rapid flood mapping: Taking advantage of EO big data. *Remote Sensing of Environment*, 209, 712–730
- Chuvieco, E., Aguado, I., Yebra, M., Nieto, H., Salas, J., Martín, M. P., ... & De La Riva, J. (2010). Development of a framework for fire risk assessment using remote sensing and geographic information system technologies. *Ecological Modelling*, 221(1), 46–58.
- Cian, F., Marconcini, M., Ceccato, P., & Giupponi, C. (2018). Flood depth estimation by means of high-resolution SAR images and lidar data. *Natural Hazards & Earth System Sciences*, 18(11), 3063–3084.
- Costabile, P., & Macchione, F. (2012). Analysis of one-dimensional modeling for flood routing in compound channels. *Water Resources Management*, 26, 1065–1087.
- D'Addabbo, A., Refice, A., Lovergine, F. P., & Pasquariello, G. (2017). DAFNE: A Matlab toolbox for Bayesian multi-source remote sensing and ancillary data fusion, with application to flood mapping. *Computers & Geosciences*, 122, 64–75.
- de Bruijn, J. A., de Moel, H., Jongman, B., Wagemaker, J., & Aerts, J. C. (2018). TAGGS: Grouping tweets to improve global geoparsing for disaster response. *Journal of Geovisualization and Spatial Analysis*, 2(1), 2.
- Defina, A. (2000). Two dimensional shallow flow equations for partially dry areas. *Water Resources Research*, 36, 3251–3264 <http://dx.doi.org/10.1029/2000WR900167>.
- Di Baldassarre, G., Castellarin, A., & Brath, A. (2009). Analysis of the effects of levee heightening on flood propagation: example of the River Po, Italy. *Hydrological sciences journal*, 54(6), 1007–1017.
- Di Baldassarre, G., & Montanari, A. (2009). Uncertainty in river discharge observations: A quantitative analysis. *Hydrology and Earth System Sciences*, 13, 913–921.
- Di Baldassarre, G., Schumann, G., Bates, P. D., Freer, J. E., & Beven, K. J. (2010). Flood-plain mapping: A critical discussion of deterministic and probabilistic approaches. *Hydrological Sciences Journal*, 55(3), 364–376.
- Domeneghetti, A., Vorogushyn, S., Castellarin, A., Merz, B., & Brath, A. (2013). Probabilistic flood hazard mapping: Effects of uncertain boundary conditions. *Hydrology and Earth System Sciences*, 17, 3127–3140.
- Dottori, F., Di Baldassarre, G., & Todini, E. (2013). Detailed data is welcome, but with a pinch of salt: Accuracy, precision, and uncertainty in flood inundation modeling. *Water Resources Research*, 49, 6079–6085.
- Emanuel, K. (2017). Assessing the present and future probability of Hurricane Harvey's rainfall. *Proceedings of the National Academy of Sciences*, 114(48), 12681–12684.
- Falter, D., Vorogushyn, S., Lhomme, J., Apel, H., Gouldby, B., & Merz, B. (2013). Hydraulic model evaluation for large-scale flood risk assessments. *Hydrological Processes*, 27, 1331–1340. <https://doi.org/10.1002/hyp.9553>.
- Ferretti, A., Prati, C., & Rocca, F. (2001). Permanent scatterers in SAR interferometry. *IEEE Transactions on Geoscience and Remote Sensing*, 39(1), 8–20.
- Filonenko, A., Hernández, D. C., Seo, D., & Jo, K. H. (2015). Real-time flood detection for video surveillance. In *IECON 2015-41st annual conference of the IEEE industrial electronics society* (pp. 004082–004085).
- Fohringer, J., Dransch, D., Kreibich, H., & Schröter, K. (2015). Social media as an information source for rapid flood inundation mapping. *Natural Hazards and Earth System Sciences*, 15(12), 2725–2738.
- Giustarini, L., Hostache, R., Matgen, P., Schumann, G. J. P., Bates, P. D., & Mason, D. C. (2013). A change detection approach to flood mapping in urban areas using TerraSAR-X. *IEEE Transactions on Geoscience and Remote Sensing*, 51(4), 2417–2430.
- Grigg, N. S., & Helweg, O. J. (1975). State-of-the-art of estimating flood damage in URBAN areas 1. *JAWRA Journal of the American Water Resources Association*, 11(2), 379–390.

- Grimaldi, S., Petroselli, A., Arcangeletti, E., & Nardi, F. (2013). Flood mapping in ungauged basins using fully continuous hydrologic-hydraulic modeling. *Journal of Hydrology*, *487*, 39–47.
- Havas, C., Resch, B., Francalanci, C., Pernici, B., Scalia, G., Fernandez-Marquez, J. L., ... Kirsch, B. (2017). E2mc: Improving emergency management service practice through social media and crowdsourcing analysis in near real time. *Sensors*, *17*(12), 2766.
- Horritt, M., & Bates, P. (2001). Effects of spatial resolution on a raster based model of flood flow. *Journal of Hydrology*, *253*, 239–249. [http://dx.doi.org/10.1016/S0022-1694\(01\)00490-5](http://dx.doi.org/10.1016/S0022-1694(01)00490-5).
- Howe, J., (2006). The rise of crowdsourcing. *Wired magazine*, *14*(6), 1–4.
- Hunter, N. M., Bates, P. D., Neelz, S., Pender, G., Villanueva, I., Wright, N. G., ... & Crossley, A. J., (2008). Benchmarking 2D hydraulic models for urban flood simulations. In *Proceedings of the institution of civil engineers: water management* (Vol. 161, No. 1, pp. 13–30). Thomas Telford (ICE publishing).
- Irwin, K., Beaulne, D., Braun, A., & Fotopoulos, G. (2017). Fusion of SAR, optical imagery and airborne LiDAR for surface water detection. *Remote Sensing*, *9*(9), 890.
- Joseph, K., Landwehr, P. M., & Carley, K. M. (2014). An approach to selecting keywords to track on twitter during a disaster. In *ISCRAM*.
- Jung, Y., & Merwade, V. (2015). Estimation of uncertainty propagation in flood inundation mapping using a 1-D hydraulic model. *Hydrological Processes*, *29*(4), 624–640.
- Leandro, J., Chen, A. S., Djordjević, S., & Savić, D. A. (2009). Comparison of 1D/1D and 1D/2D coupled (sewer/surface) hydraulic models for urban flood simulation. *Journal of Hydraulic Engineering*, *135*(6), 495–504.
- Li, Q. (2017). Characteristics and social impact of the use of social media by Chinese Dama. *Telematics and Informatics*, *34*(3), 797–810.
- Li, Z., Wang, C., Emrich, C. T., & Guo, D. (2018). A novel approach to leveraging social media for rapid flood mapping: A case study of the 2015 South Carolina floods. *Cartography and Geographic Information Science*, *45*(2), 97–110.
- Liand, Q., Borthwick, A. G. L., & Stelling, G. (2014). Simulation of dam and dyke-break hydrodynamics on dynamically adaptive quadtree grids. *International Journal for Numerical Methods in Fluids*, *46*, 127–162.
- Liu, X., Sahli, H., Meng, Y., Huang, Q., & Lin, L. (2017). Flood inundation mapping from optical satellite images using spatio-temporal context learning and modest AdaBoost. *Remote Sensing*, *9*(6), 617.
- Lopez-Fuentes, L., Rossi, C., & Skinnemoen, H. (2017, December). River segmentation for flood monitoring. In *2017 IEEE international conference on big data (Big Data)* (pp. 3746–3749). IEEE.
- MacEachren, A. M., Jaiswal, A., Robinson, A. C., Pezanowski, S., Savelyev, A., Mitra, P., Zhang, X., and Blanford, J., (2011). Sense-Place2: GeoTwitter analytics support for situational awareness, In *2011 IEEE conference on visual analytics science and technology (VAST)* (pp. 181–190), Providence, Rhode Island, USA. <https://doi.org/10.1109/VAST.2011.6102456>.
- Mandlbürger, G., Hauer, C., Höfle, B., Habersack, H., & Pfeifer, N. (2009). Optimisation of LiDAR derived terrain models for river flow modelling. *Hydrology and Earth System Sciences*, *13*, 1453–1466. <https://doi.org/10.5194/hess-13-1453-2009>
- Mason, D. C., Cobby, D. M., Horritt, M. S., & Bates, P. D. (2003). Floodplain friction parameterization in two-dimensional river flood models using vegetation heights derived from airborne scanning laser altimetry. *Hydrological processes*, *17*(9), 1711–1732.
- Mazzoleni, M., Bacchi, B., Barontini, S., Di Baldassarre, G., Pilotti, M., & Ranzi, R. (2014). Flooding hazard mapping in floodplain areas affected by piping breaches in the Po River, Italy. *Journal of Hydrologic Engineering*, *19*(4), 717–731.
- McMillan, H., & Brasington, J. (2007). Reduced complexity strategies for modelling urban floodplain inundation. *Geomorphology*, *90*, 226–243 <http://dx.doi.org/10.1016/j.geomorph.2006.10.031>.
- Mignot, E., Paquier, A., & Haider, S. (2006). Modeling floods in a dense urban area using 2D shallow water equations. *Journal of Hydrology*, *327*(1), 186–199.
- Mingham, C. G., & Causon, D. M. (1998). A high resolution finite volume method for the shallow water equations. *Journal of Hydraulic Engineering ASCE*, *124*(6), 605–614.
- Morstatter, F., Kumar, S., Liu, H., & Maciejewski, R., (2013). Understanding twitter data with TweetXplorer, in *Proceedings of the 19th ACM SIGKDD international conference on knowledge discovery and data mining, KDD '13* (pp. 1482–1485), ACM, New York, NY, USA. <https://doi.org/10.1145/2487575.2487703>.
- Neal, J., Odoni, N., Trigg, M., Freer, J., Garcia-Pintado, J., Mason, D., ... Bates, P. (2015). Efficient incorporation of channel cross-section geometry uncertainty into regional and global scale flood inundation models. *Journal of Hydrology*, *529*, 169–183. <https://doi.org/10.1016/j.jhydrol.2015.07.026>.
- Neal, J., Schumann, G., & Bates, P. (2012). A subgrid channel model for simulating river hydraulics and floodplain inundation over large and data sparse areas. *Water Resources Research*, *48*, W11506. <https://doi.org/10.1029/2012WR012514>.
- NWS. (2017). Major Hurricane Harvey.
- Omrani, E., & Sharif, H. O. (2018). Evaluation of the global precipitation measurement (GPM) satellite rainfall products over the lower Colorado River basin, Texas. *JAWRA Journal of the American Water Resources Association*, *54*(4), 882–898.
- Orton, P., Georgas, N., Blumberg, A., & Pullen, J. (2012). Detailed modeling of recent severe storm tides in estuaries of the New York City region. *Journal of Geophysical Research: Oceans*, *117*(C9).
- Poser, K., & Dransch, D. (2010). Volunteered geographic information for disaster management with application to rapid flood damage estimation. *Geomatica*, *64*(1), 89–98.
- Proust, S., Bousmar, D., Riviere, N., Paquier, A., & Zech, Y. (2010). Energy losses in compound open channels. *Advances in Water Resources*, *33*, 1–16.
- Pulvirenti, L., Chini, M., Pierdicca, N., & Boni, G. (2016). Use of SAR data for detecting floodwater in urban and agricultural areas: The role of the interferometric coherence. *IEEE Transactions on Geoscience and Remote Sensing*, *54*(3), 1532–1544.
- Refice, A., Capolongo, D., Pasquariello, G., D'Addabbo, A., Bovenga, F., Nutricato, R., ... Pietranera, L. (2014). SAR and InSAR for flood monitoring: Examples with COSMO-SkyMed data. *IEEE Journal of Selected Topics in Applied Earth Observations and Remote Sensing*, *7*(7), 2711–2722.

- Richards, J. A., Woodgate, P. W., & Skidmore, A. K. (1987). An explanation of enhanced radar backscattering from flooded forests. *International Journal of Remote Sensing*, 8(7), 1093–1100.
- Rogstadius, J., Kostakos, V., & Laredo, J. (2011). Towards real-time emergency response using crowd supported analysis of social media. In *Proceedings of CHI workshop on crowdsourcing and human computation, systems, studies and platforms* (pp. 1–3), Vancouver, British Columbia, Canada.
- Rosser, J. F., Leibovici, D. G., & Jackson, M. J. (2017). Rapid flood inundation mapping using social media, remote sensing and topographic data. *Natural Hazards*, 87(1), 103–120.
- Royapoor, M., & Roskilly, T. (2015). Building model calibration using energy and environmental data. *Energy and Buildings*, 94, 109–120.
- Sakaki, T., Okazaki, M., & Matsuo, Y., (2010). Earthquake shakes twitter users: Real-time event detection by social sensors, in: *Proceedings of the 19th international conference on world-WideWeb, WWW'10* (pp. 851–860), ACM, New York, NY, USA. <https://doi.org/10.1145/1772690.1772777>.
- Sanders, B., Schubert, J., & Gallegos, H. (2008). Integral formulation of shallow-water equations with anisotropic porosity for urban flood modeling. *Journal of Hydrology*, 362, 19–38. <https://doi.org/10.1016/j.jhydrol.2008.08.009>.
- Scalia, G., (2017). *Network-Based Content Geolocation on Social Media for Emergency Management*. Master's Thesis, Politecnico di Milano, Milan, Italy.
- Schumann, G., Bates, P. D., Horritt, M. S., Matgen, P., & Pappenberger, F. (2009). Progress in integration of remote sensing-derived flood extent and stage data and hydraulic models. *Reviews of Geophysics*, 47(4), RG4001. <https://doi.org/10.1029/2008RG000274>.
- Şen, Z. (2008). Instantaneous runoff coefficient variation and peak discharge estimation model. *Journal of Hydrologic Engineering*, 13(4), 270–277.
- Smith, L., Liang, Q., James, P., & Lin, W. (2017). Assessing the utility of social media as a data source for flood risk management using a real-time modelling framework. *Journal of Flood Risk Management*, 10(3), 370–380.
- Sun, W., Sun, Y., Li, X., Wang, T., Wang, Y., Qiu, Q., & Deng, Z. (2018). Evaluation and correction of GPM IMERG precipitation products over the capital circle in Northeast China at multiple spatiotemporal scales. *Advances in Meteorology*, 2018, 1–14.
- Tan, M. L., & Santo, H. (2018). Comparison of GPM IMERG, TMPA 3B42 and PERSIANN-CDR satellite precipitation products over Malaysia. *Atmospheric Research*, 202, 63–76.
- Tauro, F., Olivieri, G., Petroselli, A., Porfiri, M., & Grimaldi, S. (2016). Flow monitoring with a camera: A case study on a flood event in the Tiber River. *Environmental Monitoring and Assessment*, 188(2), 118.
- Toro, E. F. (2001). *Shock-capturing methods for free-surface shallow flows*. Chichester: John Wiley & Sons.
- Van Oldenborgh, G. J., Van Der Wiel, K., Sebastian, A., Singh, R., Arrighi, J., Otto, F., ... Cullen, H. (2017). Attribution of extreme rainfall from Hurricane Harvey, August 2017. *Environmental Research Letters*, 12(12), 124009.
- Viero, D., Peruzzo, P., Carniello, L., & Defina, A. (2014). Integrated mathematical modeling of hydrological and hydrodynamic response to rainfall events in rural low-land catchments. *Water Resources Research*, 50, 5941–5957. <https://doi.org/10.1002/2013WR014293>.
- Wang, R. Q., Mao, H., Wang, Y., Rae, C., & Shaw, W. (2018). Hyper-resolution monitoring of urban flooding with social media and crowdsourcing data. *Computers & Geosciences*, 111, 139–147.
- Yin, J., Lampert, A., Cameron, M., Robinson, B., & Power, R. (2012). Using social media to enhance emergency situation awareness. *IEEE Intelligent Systems*, 27, 52–59. <https://doi.org/10.1109/MIS.2012.6>.
- Yu, D., & Lane, S. (2006). Urban fluvial flood modelling using a two-dimensional diffusion-wave treatment. Part 2: Development of a sub-grid-scale treatment. *Hydrological Processes*, 20, 1567–1583. <https://doi.org/10.1002/hyp.5936>.

How to cite this article: Scotti V, Giannini M, Cioffi F. Enhanced flood mapping using synthetic aperture radar (SAR) images, hydraulic modelling, and social media: A case study of Hurricane Harvey (Houston, TX). *J Flood Risk Management*. 2020;e12647. <https://doi.org/10.1111/jfr3.12647>